2020

The Mechanics of the Bicycle Pedal Photoisomerization in Crystalline *cis,cis*-1,4-Diphenyl-1,3-butadiene

Cody R. Aldaz
University Of Michigan

Todd J. Martínez
Stanford University

Paul M. Zimmerman
University of Michigan

Aldaz, Cody R.; Martínez, Todd J.; and Zimmerman, Paul M., "The Mechanics of the Bicycle Pedal Photoisomerization in Crystalline *cis,cis*-1,4-Diphenyl-1,3-butadiene" (2020). *The Journal of Physical Chemistry A*. 25.
https://doi.org/10.1021/acs.jpca.0c05803

The Mechanics of the Bicycle Pedal Photoisomerization in Crystalline cis,cis-1,4-diphenyl-1,3-butadiene

Cody R. Aldaz, Todd J. Martínez, and Paul M. Zimmerman

Abstract

Direct irradiation of crystalline cis,cis-1,4-diphenyl-1,3-butadiene (cc-DPB) forms trans,trans-1,4-diphenyl-1,3,-butadiene via a concerted two bond isomerization called the bicycle pedal mechanism. However, little is known about photoisomerization pathways in the solid-state and there has been much debate surrounding the interpretation of volume-conserving isomerization mechanisms. The bicycle pedal photoisomerization is investigated using the QM/MM complete active space self-consistent field (CASSCF)/Amber force-field method. Important details about how the steric environment influences isomerization mechanisms are revealed including how the one-bond flip and hula-twist mechanisms are suppressed by the crystal cavity, the nature of the seam space in steric environments, and the features of the bicycle pedal mechanism. Specifically, in the bicycle pedal the phenyl rings of cc-DPB are locked in place and the intermolecular packing allows passageway for rotation of the central diene in a volume-conserving manner. In contrast, the bicycle pedal rotation in the gas-phase is not a stable pathway, so single-bond rotation mechanisms become operative instead. The present models, however, do not capture the quantitative activation barriers and more work is needed to better model reactions in crystals. Lastly, the reaction barriers of the different crystalline conformations within the unit cell of cc-DPB are compared to investigate the possibility for conformation-dependent isomerization. Although some difference in reaction barriers are observed, the difference is most likely not responsible for the experimentally observed periods of fast and slow conversion.

Introduction

The ability of light to trigger mechanical changes via photoisomerization is well known in vision and phototaxy, driving efforts to replicate these features in artificial molecular machines and

optomechanical devices. This has led to the study of specific isomerization mechanisms such as one-bond flip (OBF, also known as the double-bond twist), volume-conserving hula-twist (HT), and the bicycle pedal (BP) mechanisms[1]. The relative importance of these photoisomerization steps in condensed phases, however, is particularly sensitive to the steric environment. Furthermore, the study of these mechanisms is notoriously difficult because thermal isomerization about carbon-carbon single bonds can mix the photoproducts. As a result, many questions and debate[2–6] surround the interpretation of photoisomerization mechanisms, and this confusion inhibits rational design.

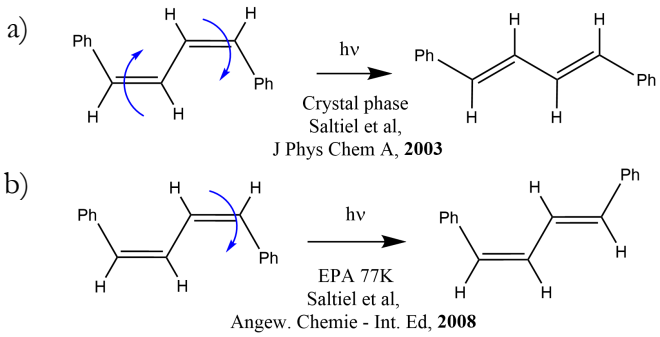

Figure 1 Irradiation of cc-DPB in different steric environments results in different isomerization products a) crystal b) viscous environment.

Herein, the isomerization of crystalline cis,cis-1,4-diphenyl-1,3-butadiene (cc-DPB),[7,8] to trans,trans-1,4-diphenyl-1,3-butadiene (tt-DPB) is investigated (Figure 1a). This isomerization may proceed through the concerted BP mechanism, which has been noted in crystalline butadienes[9–11,12] (some of which produce macroscopic motion like peeling[12]), hexatrienes[13,14], photoactive yellow protein[15], and has been implicated in the visual retinoid cycle[16]. Photoirradiation of crystalline cc-DPB is interesting among these because in solution and glassy phase the BP isomerization is minor or absent. For example, photoirradiation of cc-DPB in ethanol[17] produces ct-DPB via OBF (or HT), and a minor amount of tt-DPB through a phenylallylbenzyl intermediate, not through concerted rotation as portrayed in the BP mechanism[17]. Furthermore, cc-DPB in viscous media like glassy phases mostly does not undergo BP isomerization: photoirradiation in the viscous isopentane glass resulted in a mixture of single double-bond isomerization and BP isomerization[7], whereas photoirradiation in the harder EPA (ether:isopentane:ethyl alcohol=5:5:2) glass resulted in no BP isomerization(Figure 1b)[18]. This is unexpected because isomerization in volume-restricting environments is generally expected to proceed via the more volume-conserving mechanism (e.g. HT/BP vs OBF)[1]. These observations therefore suggest that specific steric and structural interactions must be present in the crystal which inhibit the single double-bond isomerization and enable the BP pathway.

In order to gain more information into this intriguing mechanism, it is useful to perform *ab initio* computational analysis. Previous studies on related compounds[19–25] have demonstrated that

quantum chemical simulations can provide important details of photoisomerization mechanisms that would be useful for understanding cc-DPB photochemistry. Specifically, conical intersections (crossings between potential energy surfaces) enable efficient non-radiative decay between states, and therefore control photoproduct formation. Quantum mechanical studies of conical intersections responsible for the BP mechanism, however, are to the best of our knowledge unexplored. Furthermore, the investigation of reaction mechanisms in crystal environments is more difficult than their gas-phase counterparts. Zimmerman was the first to report *ab initio* investigations of crystal photochemical reactions by approximating crystal packing with an inert gas-shell model[26]. Later, the same author optimized cluster models using a quantum mechanics/molecular mechanics (QM/MM) ONIOM approach[27,28]. Recent advances in related techniques applied to crystal photochemistry[29,30] have permitted improved geometry optimization as well as better treatment of short-range[31] and long-range electrostatic effects[32,33] in crystals with quantum mechanics/quantum mechanics' methods (QM/QM') methods.

In this article, a recently developed reaction path optimization method[34,35] is applied to analyze photoisomerization of cc-DPB. First, analysis of traditional OBF double-bond isomerization pathways provides insight into why these pathways are forbidden in crystals. Details of the BP mechanism for DPB in crystal are then revealed for the first time. The descriptions of these pathways will reveal how the crystal phase affects conical intersections and on how the broader seam topography depends on restrictions on intramolecular rotation. Finally, a hypothesis about the isomerization rate varying on a conformer-specific level is evaluated[8,36,37]. Altogether, this information provides a close look at the effects of environment on photoisomerization mechanisms and explains how qualitative changes in reaction pathways can come with entry of molecules into the crystal phase.

Methods:

Cluster model

The cc-DPB crystal structure was retrieved from the Cambridge crystal database (CIF #29021)[7]. A 3x3x3 cluster was prepared and a four-layer QM/MM approach was utilized for all calculations unless otherwise stated (Figure 2). Ordinarily, there are three layers in the crystal cluster models: QM, MM, and MM frozen[27,28]. An extra layer arises here because of the hybrid Cartesian and translation-rotation internal coordinate (TRIC) system which enables efficient coordinate

optimization and transformation (see below)[35]. The choice of layers is as follows. The first layer contains the QM molecule, which depends on the specific conformation of the unit cell being investigated (see below). The second layer is defined as all monomers with all atoms less than 5 Å from the QM monomer and is treated with MM and TRIC. The third layer is defined as monomers with all atoms greater than 5 Å away from the QM monomer and less than 10 Å from the QM monomer and is treated with MM and Cartesians. The fourth layer is all monomers with all atoms greater than 10 Å from the QM monomer; this layer is kept frozen and is treated with Cartesian coordinates. The QM layer is treated with the state-averaged complete active space self-consistent field (SA-CASSCF) method. All layers besides the QM layer are treated with the Amber14 force field and utilize restrained electrostatic potential charges (RESP) derived from quantum mechanics. The atom types and charges are provided in the **Supporting Information**. The choice of active space in the SA-CASSCF is discussed below because that requires further experimental and theoretical considerations.

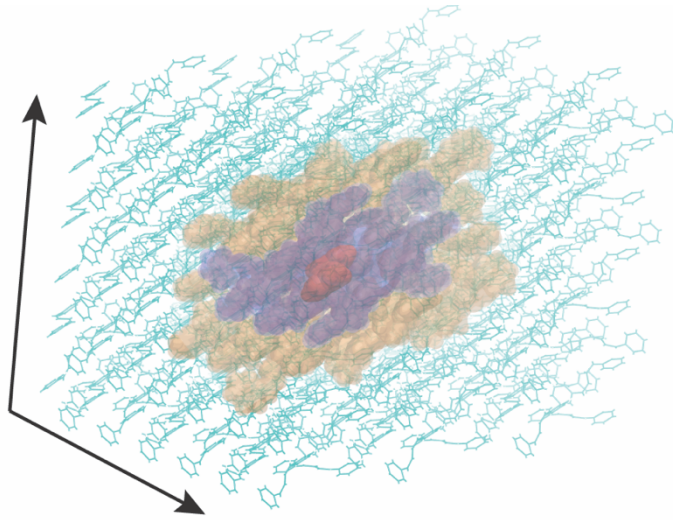

Figure 2. 3x3x3 cluster model of cc-DPB. The colors represent the four-layer geometry optimization approach. Red VDW: non-frozen QM region treated with TRIC, blue VDW: non-frozen MM region treated with TRIC, transparent VDW orange: non-frozen MM region treated with Cartesians, line cyan: frozen MM region treated with Cartesians. There are 12960 atoms total.

The use of frozen atom boundary conditions was investigated by comparing the BP pathway (cc-DPB→tt-DPB) in the ground-state with and without frozen boundary conditions using the MM level of theory (**Supporting Information**). No significant difference in the ground-state BP pathway was observed for the frozen-atom vs no frozen atom simulation. Therefore, because the present implementation of QM/MM must rely on frozen boundary conditions or some other type of restraints to maintain crystal packing, freezing the outer layer of the crystal is not expected to affect the excited-state QM/MM simulations.

Reaction Path Optimization

Reaction path optimization was performed with the growing string method (GSM) as implemented in Python3[38]. The core GSM algorithm has been described separately[39,40], and

modifications necessary to treat large systems will be described in detail elsewhere[34]. Therefore, only a brief description is given here. GSM is an efficient reaction path optimization algorithm that can be operated in either single-ended or double-ended mode. Single-ended mode requires an initial structure and a driving coordinate direction (e.g. adding or breaking bond) and is therefore well suited for reaction discovery and exploration[41]. This mode has also been shown to be useful for finding MECI starting from stable equilibrium geometries[42]. The double-ended mode requires an initial and final structure as input. GSM employs delocalized internal coordinates (DLCs) which are superior to Cartesian coordinates for geometry optimization[43]. In the present implementation of GSM, translation and rotation internal coordinates (TRIC)[35] are used to reduce the computational cost of coordinate transformations. With the inclusion of TRIC, the individual molecules of the cluster are decoupled and therefore block-matrix diagonalization techniques are used to achieve linear scaling (in the number of molecules, N_{mol}) computational cost[34]. Further reductions in cost for coordinate transformation are obtained by treating a subset of the atoms with Cartesian coordinates (see **Supporting Information**).

Python GSM is available for free on Github[38] and is interfaced with GPU-accelerated TeraChem for QM and QM/MM calculations[44–46], and OpenMM for MM calculations[47]. Initial geometry optimization of the 3x3x3 crystal was performed with OpenMM without the frozen constraints to relax the MM region. MECI optimization was performed using an iterative penalty potential[48]. Gradient RMS, gradient maximum, and energy difference criteria were used to determine optimization convergence. Transition state optimization was performed using a climbing image algorithm[39]. The transition states are considered optimized when the gradient RMS and reaction tangent are converged to 0.0005 Ha/(Bohr rad), and the difference in energy between successive iterations was less than 0.1 kcal/mol. Seam saddle point were optimized with climbing image optimization using the same criteria, on the penalty potential with σ of 10.

Complete active space self-consistent field

Photoisomerization can proceed through crossings between potential energy surfaces, which requires electronic structure theory that can treat electronic degeneracies[49]. The CASSCF method is therefore a workhorse in the study of photoisomerization and photochemical reactions. Previous computations on 1-phenyl-1,3-butadiene have analyzed the potential energy surface with the SA2-CAS(10,10)SCF/6-31+G* level of theory, including the 10 carbon p orbitals involved in π-bonding[22]. These computations showed the excited state is more planar due to increased coupling between the

phenyl and diene moiety, and a low energy (3 kcal mol^{-1} higher than the S_1 minimum) conical intersection was found leading to a spiro-cyclization photoproduct, which agrees with available experimental data. In contrast, the isomerization pathways were found to be much higher at about 25 kcal mol^{-1} above the S_1 minimum. The isomerization MECI can be described as *s-transoid* (s-trans with respect to the phenyl diene single bond), and a *central* MECI by analogy with butadiene[19].

Butadiene has also been extensively studied and it has been found that SA-CASSCF with the nonintuitive active space of four electrons in three orbitals closely approximates both second order MS-CAS(4,4)PT2[50] and experiment. This choice of active space destabilizes the S_1 surface while leaving the S_2 surface largely unchanged, restoring the near-degeneracy of S_2 and S_1 in the Franck-Condon region. The *transoid* MECI is about 39 kcal mol^{-1} below the Franck Condon point, the S_1 minimum of butadiene is a twisted methylene. At the higher SA-3-(4,4)-MSPT2/6-31G** level of theory [21] the *transoid* MECI is about 22 kcal mol^{-1} below the planar 2 ^1A_g state, and 41.5 kcal mol^{-1} below the Franck-Condon point.

The full π space of cc-DPB requires a (16,16) active space which is at the high-end of computational capabilities, especially for the relaxed reaction path optimization performed herein. Furthermore, a larger active space is not always better, and this is perhaps evident in 1-phenyl-1,3-butadiene that has a large isomerization barrier at the SA2-CAS(10,10) level. Therefore, for an initial investigation it is reasonable to begin with a smaller active space. To our satisfaction, the SA3-CAS(4,3)SCF captures spectroscopic characteristics in agreement with SA3-(4,4,)-MS-PT2 calculations. The bright, ionic S_1 state has B_u-like symmetry in agreement with experiment[51], and, like PB[22], is described as bichromophoric (see **Supporting Information**). The dark, covalent S_2 state has A_g symmetry and is approximately 1 eV (23 kcal/mol) above the S_1 state. Experiments place the S_2 state of tt-DPB 3.3 kcal/mol below the 1 ^1B_u state in the gas-phase, but the $1^1B_u \rightarrow 1^1A_g$ transition energy decreases with increasing medium polarizability; for example, S_1 is the 1^1B_u state in all hydrocarbon solvents[51]. Furthermore, these experiments on tt-DPB observe that the isomerization occurs via the 1^1B_u state[51]. Note that this is different than butadiene where the covalent 2^1A_g state is below the ionic 1^1B_u state, and the trans/cis isomerization is preceded by passageway through the $1^1B_u/2^1A_g$ (S_2/S_1) conical intersections[50]. Therefore, SA3-CAS(4,3)SCF qualitatively reproduces key features of the experiment[51]. The SA3-CAS(4,4)SCF level, in contrast, does not agree with the MS-PT2 calculations, it predicts S_2 as the bright state and the excitation is localized on the butadiene chromophore.

Results and Discussion

The analysis of cc-DPB photoisomerization pathways begins with a brief description of the crystal and gas-phase ground- and excited-state structures. Next, single double-bond isomerization mechanisms are revealed, with details about why these are prohibited in the crystal. Then a comprehensive analysis of BP pathways is provided. Finally, the BP reaction paths for all conformers within the unit crystal are compared to determine if certain conformations isomerize with faster rates than others.

Crystal Description

Table 1 CASSCF excitation energies in eV, (CASPT2 energies of the monomer in gas-phase)

Geometry	ΔE_{vert}	ΔE_{adiab}
A isomer	5.942	4.468 (3.794)
B isomer	6.000	4.600 (3.767)
C isomer	5.827	4.250 (3.562)
D isomer	6.050	4.453 (3.771)
Perpendicular Vacuum	5.727	4.317
Parallel Vacuum	7.513*	4.175

The cc-DPB unit cell contains two conformers of the monomer, for a total of four DPB molecules. One of the conformers has the phenyls in perpendicular planes (**A**,**B**) and the other has phenyls in parallel planes (**C**,**D**), see Figure 3. The two conformers of cc-DPB arrange in edge-to-face alternating arrays: the perpendicular conformers clasp together in a row of the array, and the parallel conformers clasp together in the next row of the array. The parallel and perpendicular conformers are also stable geometries in the gas phase. In the gas phase the angle of the diene with respect to the phenyl planes is 90°, compared to the crystal angles of ~45°.

* C_{2h} symmetry

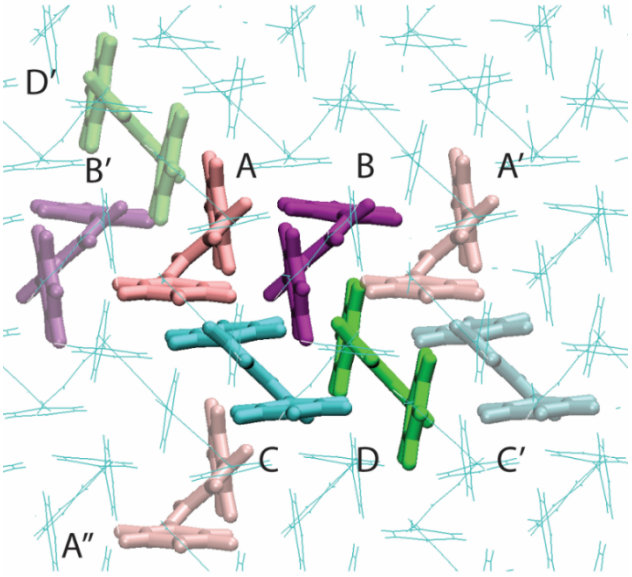

Figure 3. Unit cell with labels. Cyan: A, Purple: B, Red: C, Green D. The lighter colored monomers are members of adjacent cells, which interact with the central conformers.

The calculated vertical and adiabatic excitation energies of each of the conformers in the crystal phase and gas-phase are reported in Table 1. The experimental vertical and adiabatic excitation energies can be estimated from the excitation and emission spectrum, respectively, and are approximately 3.387 eV (366 nm) and 3.024 eV (410 nm)[8]. In contrast, in cyclohexane solution the vertical and adiabatic excitation energies are 4.27 eV (290 nm) and 3.56 eV (360 nm)[51]. Therefore, the crystal exhibits a strong bathochromic shift with respect to solution, which is known to arise from the long-range electrostatic effects in crystals[32,33]. The CASSCF results show significantly higher excitation energies, due to the well-known lack of dynamical electron correlation. CASPT2, which includes dynamical electron correlation, brings the energies closer in line with solution values, but does not account for the environmental effects of the bulk crystal.

OBF Double Bond Rotation

The photoisomerizations of conformer **C** were examined first because this conformer has the lowest energy initial excited state. Two *cis,cis-s-transoid* MECIs were found, where the *s-trans* nomenclature is with respect to the central single bond. These MECI are labeled as *cc-transoid-L* and *cc-transoid-R* because they resemble the rotation of the left and right side of a bicycle pedal, respectively (top row Figure 4, and Table 2). To understand how the crystal steric environment affects these MECI, the gas-phase MECIs were also found. The structures are overlaid to show how the crystal affects the geometry, and the MECI energies are shown in the color matching the conformer (e.g. dark blue for gas phase). The crystalline *cc-transoid* MECI differ from the gas phase, in that they are higher in energy than their respective S_1 minimum by 6.6 and 13.1 kcal mol^{-1} for *cc-transoid-L* and *cc-transoid-R*, respectively[52]. The increase in energy of conical intersections from gas-phase to crystal can be explained by restrictions on intramolecular rotation (RIR)[53,54]. As can be seen in Figure 4, the gas-phase cc-*transoid* MECI are able to significantly deviate from planarity (α=43° and 51°) whereas the crystalline phenyls require less than half the amount of out-of-plane rotation, consistent with RIR. Rotating out of plane is energetically favorable in the gas phase because it helps the phenyl maintain conjugation with the rotating interior hydrogen (H4 or H5). In contrast, α is prevented from changing due to steric repulsion in the crystal.

Table 2 Single double-bond isomerization MECI energies and geometric characteristics.

MECI		S_0[a]	S_1[a]	θ[b]	φ[b]	α[b,c]
cc-transoid-L	gas-phase	-1.8	-1.7	-83.6	-130.9	42.8
	crystal-phase	6.6	6.7	-86.6	-137.7	20.6
cc-transoid-R	gas-phase	-1.8	-1.7	85.3	131.4	50.6
	crystal-phase	13.1	13.1	83.6	137	23.7
s-transoid	gas-phase	-1.4	-1.3	-69.6	-166.1	40.3
	crystal-phase	3.0	3.2	-29.5	-174.4	3.8
s-central	gas-phase	-7.0	-6.9	115.6	-173.1	120.8
	crystal-phase	-0.6	-0.6	38.0	166.8	29.1

[a] Energy in kcal/moll with respect to the local S_1-minimum.
[b] angle in degrees, see Figure 4
[c] α is defined as the angle between the planes of the phenyl and the S_1-minimum.

The MECI geometries imply the existence of specific photoproducts. Herein the gas-phase *cc-transoid* are assumed to lead to OBF and HT-2 (Figure 5) because they contain a combination of double-bond rotation (θ) and adjacent single-bond rotation (φ) coordinates (Figure 4)[24]. In the OBF mechanism the phenyl completes the ~180° twist about the carbon-carbon double bond. For example, OBF characteristics can be seen in the angle α as the phenyl group flips over C3-C4 in Figure 4. In the HT mechanism single-bond rotation about the central double bond allows the CH group (e.g. C4-H4) to complete the twist about the double bond without flipping the phenyl; α decreases as the hydrogen finishes the hula-twist. Interestingly, the perpendicular geometry α begins at ~90°, therefore

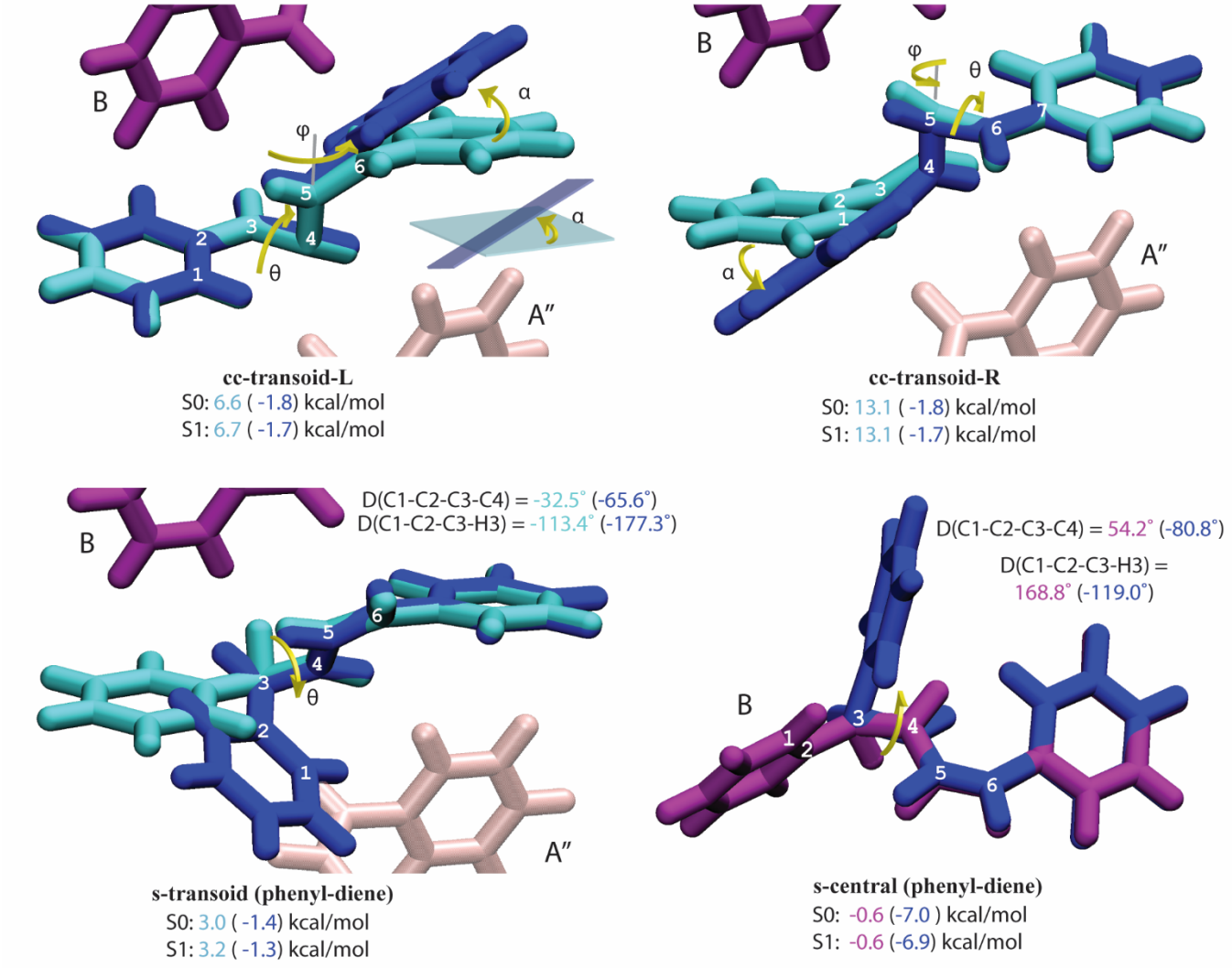

Figure 4. Geometries of gas-phase (dark blue) and crystalline transoid conical intersections (see **Figure 3**) involved in single double bond isomerization. The important coordinates are labeled one-bond flip coordinate (θ), single-bond rotation coordinate (φ) and phenyl out-of-plane angle (α). α is defined as the angle between the planes of the phenyls of the MECI and S_1 minimum. The energies and values for the different parameters are shown in the color matching the conformer: dark blue for gas-phase, cyan for **C**, purple for **B**. The S_0 and S_1 energies, in kcal mol^{-1} are relative to the respective S_1 minimum geometry.

only half the necessary phenyl rotation is required for OBF, which may facilitate OBF in the gas-phase.

The expected photoproducts in the crystal-phase, however, are much different. The *cc-transoid* MECI distortions imply that completion of the OBF and HT are no longer allowed[24]. OBF is clearly suppressed in the crystal state via restrictions on out-of-plane rotation due to the constrained cavity. Furthermore, although α is smaller in the crystal phase, rotation about the central single bond (φ) is also suppressed in the crystal lattice, and this is evident in the MECI with φ about 7° larger; a smaller φ means greater rotation. This is interesting because it shows that although HT is more volume conserving than OBF it still requires that the phenyls "slide" via the single-bond rotation coordinate φ, which is prohibited in the crystal phase.

Another class of CI important for single double-bond isomerization occurs via pyramidalization at the first carbon of the diene. Two CI[22] with pyramidalization at the first carbon can be found in the gas-phase for cc-DPB. The two differ in the dihedral phenyl-diene single bond, and can be described as *s-central* and *s-transoid* where the *s-trans* and *s-central* naming refers to the phenyl-diene single bond (Figure 4 bottom row and Table 2)[22]. These CI are assumed to lead to HT-1 and OBF photoproducts (Figure 5). The difference in photoproducts is the orientation of the resulting

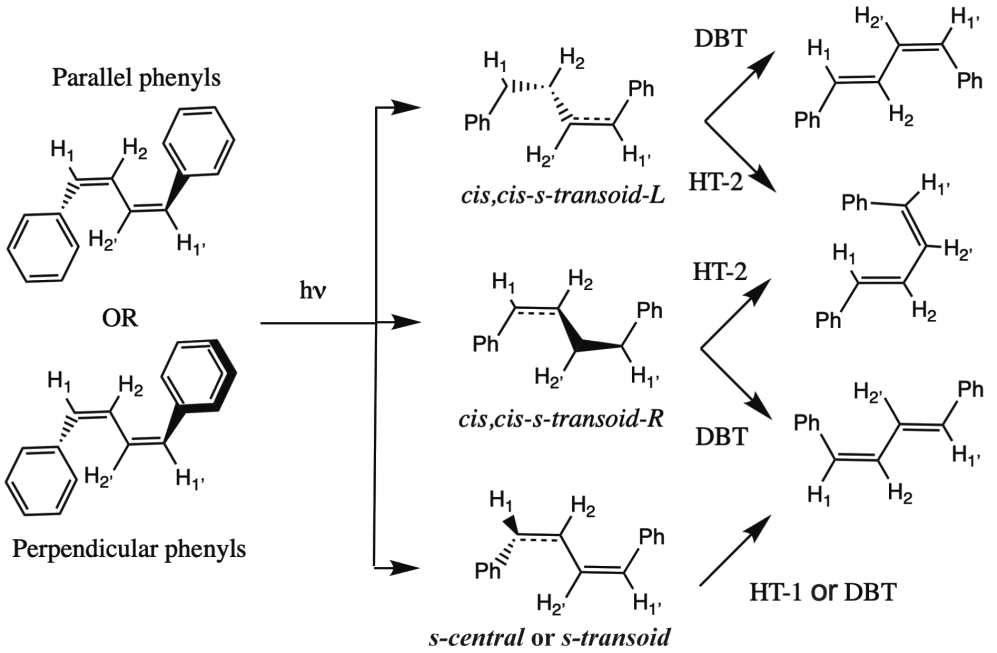

Figure 5. Single double-bond isomerization mechanisms. Operative only in the gas phase due to steric blockage in the crystal.

phenyl: in OBF the phenyl ring flips 180° about the phenyl-diene carbon-carbon single bond, whereas HT-1 preserves the relative phenyl position.

Crystal phase planar analogues of *s-transoid* and *s-central* were found starting from the parallel phenyl geometries (**C**) and perpendicular phenyl geometries (**B**), respectively. In comparison to *cc-transoid*, an even greater difference between gas phase and crystal phase exists for this pair of conical intersections. In the crystal phase, the dominant motion rotates the hydrogen out of plane, e.g. D(C1-C2-C3-H3) = -113.4° and the phenyls remain in plane (e.g. α=4°). This is unusual because rotation of hydrogen out of plane has only been found in the gas-phase as a high-energy seam saddle point[23,42,55]. In order for this conical intersection to become responsible for the HT in the condensed phase, the steric surroundings must in some way cause this conical intersection to become lower energy. This has previously been hypothesized[23,42,55], but was not tested until now due to the lack of capacity to simulate the reaction mechanism in the condensed phase, and therefore highlights the importance of explicitly modeling the steric environments: the nature of the potential energy surface topology including the seam space can change dramatically in the condensed phase. Incidentally, SE-GSM was particularly beneficial here because the gas-phase and crystal phase structures were found from the same input reaction coordinates. In contrast, the optimization of these structures via traditional techniques where the gas-phase structure is used as a guess for the reacting system of the crystal would not work because the gas-phase structures do not fit within the crystal cavity. Regardless, the crystalline *s-transoid* and *s-central* CI analogues are also non-productive in the crystal phase due to restrictions on side-to-side rotations.

Bicycle Pedal Rotation

The CI responsible for bicycle pedal isomerization in the crystal phase is now identified and analyzed. As demonstrated above, the *cc-transoid-L* and *cc-transoid-R* MECI each resemble one half-rotation of a bicycle pedal. Putting these motions together in a concerted manner completes the cycle. As can be seen in Figure 6a, the bicycle-pedal CI be described as *trans,trans-s-transoid,* or *tt-transoid* for short. As above, the gas-phase *tt-transoid* is more non-planar than the crystalline form, and this extra flexibility allows gas-phase *tt-transoid* to reach a lower energy than the crystal phase.

Excited-state reaction paths were found connecting the S_1-minimum and the *tt-transoid* CI. In the crystal state, the reaction path is a single, smooth elementary step consisting of ~180 degree rotation of the central diene, followed by pyramidalization (Figure 6b). In contrast, in the gas-phase the reaction path from the S_1-minimum to *tt-transoid* undergoes significant out-of-plane distortion as the phenyls attempt to maintain conjugation with the central rotating diene (see **Supporting Information)**. No exact transition state geometry could be optimized, probably due to the unstable (high energy) nature of the reaction path. Taken together with the steepness of the potential energy surface towards the *cc-transoid* CI in the gas-phase (Figure 4), this indicates that the BP pathway is not operable in the gas phase. The crystal BP mechanism is also considerably different than the solution-phase cc-DPB→tt-DPB mechanism which proceeds through a cis-phenylallylbenzyl excited state intermediate[17]. For example the cis-phenylallylbenzyl intermediate would require side-to-side motion of the phenyl, which is not allowed in the crystal. Therefore, the crystal state is unique in its operation: the steric environment opens the bicycle pedal isomerization reaction valley by restricting out-of-plane motion and allowing smooth rotation of the diene.

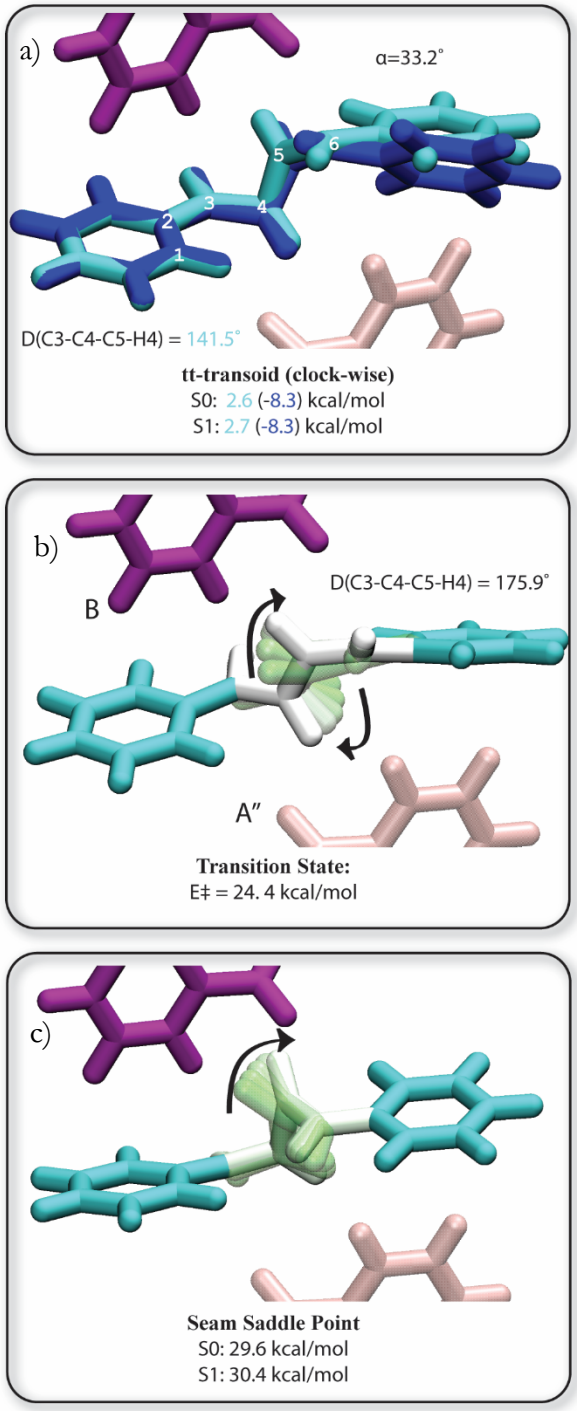

Figure 6. Relevant geometries for the bicycle pedal isomerization a) comparison of gas and crystal phase tt-transoid MECI, b) excited-state transition state connecting S_1 minimum and transoid MECI c) seam saddle point connecting cc-transoid-R and tt-transoid MECI. The S_0 and S_1 energies, in kcal mol^{-1} are relative to the S_1 minimum geometry of **C**.

Close inspection of the transition state geometry reveals additional important details. First, as can be seen in Figure 6b, the pedal rotates neatly through the phenyl-diene gaps of the adjacent **B** and **A"** molecules. The adjacent phenyls prevent out-of-plane rotation by locking the pedals into gear. Thus, the BP isomerization resembles the mechanical operation of real bicycles in more than one way: the concerted rotation, and the mechanical rigidity in being locked into this rotation pathway. Second, the transition state geometry has no pyramidalization (D(C1-C2-C3-H2)=175.9°) which indicates that the isomerization might bifurcate to tt-DPB in the excited-state. Indeed, an excited-state reaction pathway was found that connects the S_1-minimum and tt-DPB S_1-minimum with an identical transition state geometry as Figure 6b, although they were computed independently. Therefore, this shows that the transition state bifurcates to lead to the tt-DPB S_1-minimum and *tt-transoid* MECI. At the S_1-minima, the excited-molecule can decay non-radiatively at the *tt-transoid* through pyramidalization, or radiatively through fluorescence.

MECI, however, are not enough to fully describe the photochemistry because non-radiative decay can occur at any point along the high-dimensional seam-space. In particular, regions of the seam are often found parallel to the adiabatic reaction coordinate and can contribute via motion orthogonal to the reaction coordinate[56]. Therefore, to explore the potential energy surface more widely for other possible bicycle pedal mechanisms, a minimum energy seam pathway was found connecting *cc-transoid* and *tt-transoid*. This seam runs roughly parallel to the adiabatic pathway and the seam saddle point occurs near the excited-state transition state (Figure 6c). Non-radiative decay through CI points before the seam saddle point are considered to return to cc-DPB, whereas all CI points at or after the saddle point lead to tt-DPB. With this seam established a complete picture of the relevant BP potential energy surface is now known and a summary of the important pathways, productive and non-productive, is given in Figure 7.

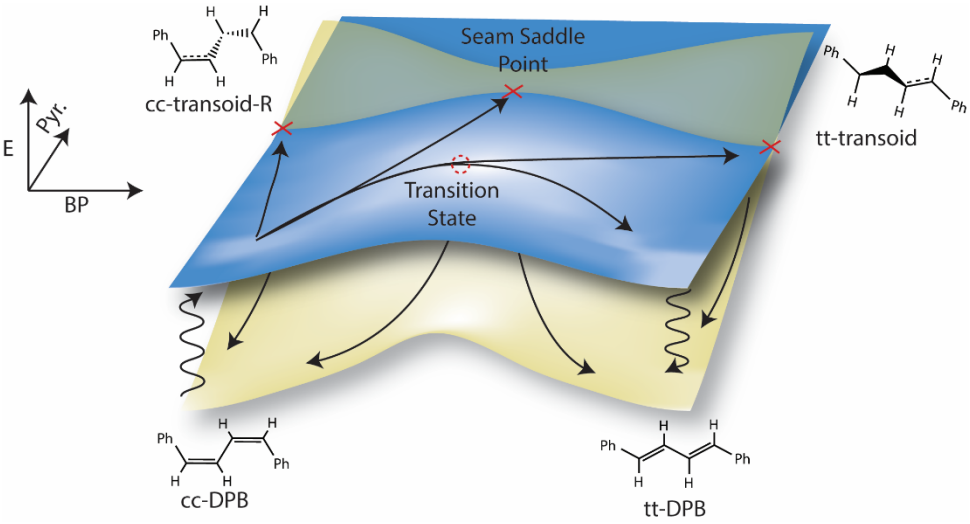

Figure 7. Summary of major excited-state reaction channels of conformer C, including productive and non-productive routes.

Figure 7 provides a summary of the proposed photoisomerization pathways. Starting from photoexcited cc-DPB conformer **C**, the transition state energy leading to the bicycle pedal CI (24.4 kcal mol^{-1}) is below the vertical excitation energy (36.3 kcal mol^{-1}) suggesting that enough energy is available to overcome the barrier (at least at short timeframes following excitation). This pathway is much lower in energy than the ground-state process (98.4 kcal mol^{-1}). However, a significant region of the seam runs roughly parallel to the adiabatic coordinate, which can drain energy from the excited-state via non-productive decay to the reactants (i.e. an aborted OBF or HT). The productive formation of tt-DPB would only start around the seam-saddle point connecting *cc-transoid* and *tt-transoid* which is much higher in energy. Nevertheless, despite the high-energy excited-state activation barrier the BP isomerization pathways appears reasonable. If the phenyls are held stationary the motion would have to be confined to the diene portion of the molecule. Furthermore, the gaps between the phenyls and diene enable unimpeded passage for CH rotation. Therefore, at present the large barrier is considered an artifact of the lack of quantitative energies provided by CASSCF (e.g. **Error! Reference source not found.**) in computing these electronic states, or long-range interactions which are not captured in the MM model. Future studies will test the accuracy of this relatively simple level of theory against higher-accuracy methods.

Conformation Comparison

Now that the mechanism for cis-trans photoisomerization in cc-DPB have been outlined, the various conformers within the unit cell are studied. Besides categorization into parallel and perpendicular units, the steric environment surrounding the central double bond of each conformer is different and could result in different activation barriers for BP isomerization. If the conformations have different activation barriers, this could help explain the experimentally observed periods of fast and slow conversion because certain conformers will isomerize with a slower rate, and therefore, with less photon efficiency[36].

Table 3. Intermolecular interactions during the bicycle pedal isomerization for each unit in the clockwise and anti-clockwise direction. See **Figure 3** for the point-of-reference used to make this table.

		Neighbor	
Conformer	Bicycle-Pedal Direction	Top Pedal*	Bottom Pedal*
A	clockwise	**B**	**B'**
	counter-clockwise	**D'**	**B**
B	clockwise	**A'**	**A**
	counter-clockwise	**A**	**D**
C	clockwise	**B**	**A''**
	counter-clockwise	**A''**	**B**
D	clockwise	**C'**	**C**
	counter-clockwise	**C**	**C'**

*Top and bottom pedal refer to central CH groups of the diene with point-of-view in Figure 3.

As we have seen, the primary motion during the BP isomerization is the rotation of the central CH groups between the phenyl-diene gap of neighboring units. The steric interaction of these "pedals" and the neighboring monomers are therefore of concern. Isomerization in the clockwise direction versus the counter-clockwise direction can also lead to differences in isomerization efficiencies, depending on conformer. To familiarize oneself with the different steric environments, consider the counter-clockwise rotations of **A** and **B** as an example. The diene of unit **A** and **B** are oriented similarly, however the steric interactions upon isomerization are different. The top pedal (CH) of **A** slips between the gap of the phenyl and diene of **D'** and the

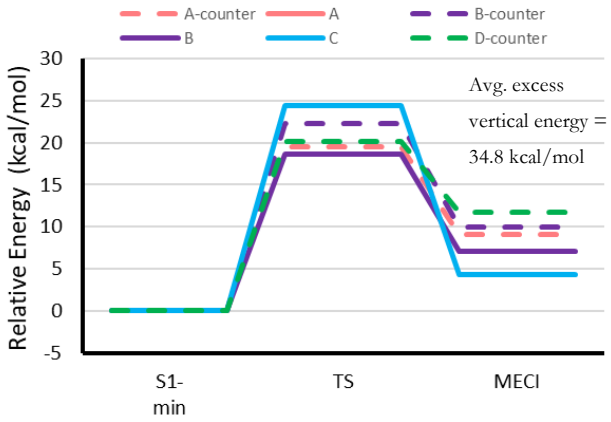

Figure 8. Comparison of bicycle pedal reaction paths to MECI for all conformers. The average vertical excess energy is over conformers A-D which have different microenvironments and energies.

bottom pedal becomes perpendicular with the phenyl of **C** and rests near **B**. On the other hand, the bottom pedal of **B** slips between the phenyl diene gap of **D** and the top pedal sterically clashes with **A**. Similar analysis has been performed for all conformers in both rotation directions, and is present in Table 3.

With all the expected interactions tabulated, excited-state reaction pathways between the S_1-minimum of each conformer and the appropriate *tt-transoid*-CI were found for clockwise and counter-clockwise rotations (Figure 8). A range of about 6 kcal/mol is observed between all conformers: conformer **B** has the lowest energy barrier of 18.6 kcal/mol in the clockwise direction, and conformer **C** has the largest barrier of 24.5 kcal/mol. Clockwise BP rotation of conformer **B** causes the top pedal to pass first through the phenyl-diene gap of **A'** and then of **D**. The bottom pedal of conformer **B** skirts past **A** and does not pass directly through a phenyl-diene gap. In contrast when **B** rotates in the counter-clockwise direction, the bottom pedal rotates through **D** and as it approaches **A'** it relaxes before going through the gap. The top pedal of conformation **C** also does not pass through the phenyl diene gap of **B** during clockwise rotation. Overall, however, these differences appear to be well within errors of the current semi-quantitative model. For all MECI and RP diagrams of these various conformers, consult the **Supporting Information**.

Nevertheless, to answer the question of whether the different conformations are responsible for different isomerization rates in the experiments (fast and then slow), the answer is most likely "no". All conformers can rotate without major impediment and the major steric interaction provided by the crystal lattice is to restrict out-of-plane rotations of the phenyl, which is present in all conformers. Furthermore, additional experiments have observed that the related compound cis,trans-1,4-di-o-tolyl-1,3-butadiene (cc-DTB) has no conformational anisotropy[11] yet also displays periods of fast and slow isomerization kinetics. As a result, it is reasonable to suggest that conformational differences are not responsible for the observed stepwise reaction rate, but instead the effect is due to more complex changes as the crystal reorganizes.

Conclusions

The present computational investigation of cc-DPB provided substantial insight into the diverse OBF, HT, and BP mechanisms in the gas-phase and crystal states. The out-of-plane angle α and the side-to-side rotation angle φ were found to be useful parameters to explain why OBF and HT were prohibited in the crystal phase. Interestingly, the crystal phase can fundamentally change the seam topology, as seen in how the HT-1 conical intersection in the crystal phase resembles gas-phase seam saddle points. The dramatic influence of the steric environment is also evident in the BP isomerization, where the phenyls are locked in place and the diene must rotate in a smooth volume-conserving manner. The specific way the monomers clasp together is also important for ensuring unimpeded passageway for the rotating diene. In contrast, cc-DPB is not able to isomerize via the BP in the gas phase because it lacks a rigid structure that is essential for ensuring a smooth rotation, without relaxation into non-BP geometries.

BP isomerization paths for unit-cell conformers revealed that all conformers isomerize in a similar fashion. This indicates that the fast and slow reaction kinetics observed in experiment are not likely to be a result of the different microenvironments in the unit cell, at least in the early stages of isomerization before the crystal reorganizes.

The growing string method was instrumental in locating the reaction pathways, conical intersections, and seam spaces throughout this study. In particular, the qualitative differences in isomerization pathways between the gas phase and solid state were straightforwardly delineated by GSM, allowing these mechanisms to be brought to light without undue reliance on prior chemical intuition. However, quantitative accuracy in describing the bicycle pedal has not yet been achieved. Therefore, in addition to providing relevant details of the BP mechanism we hope that this study can further motivate computational analysis of photochemical reactions in the solid state.

Acknowledgment

We are thankful to Professor Jack Saltiel for providing useful feedback on early drafts of this manuscript. This work is supported by NSF (CHE 1551994 to PZ) and Office of Naval Research (ONR-N0014-18-1-2659 to TJM).

Supporting Information

MM parameters, molecular orbital diagrams, and reaction path profiles are provided in the Supporting Information.

References

(1) Liu, R. S. H.; Yang, L.-Y.; Liu, J. Mechanisms of Photoisomerization of Polyenes in Confined Media. From Organic Glasses to Protein Binding Cavities. *Photochem. Photobiol.* **2006**, 2–10. https://doi.org/10.1562/2006-01-27-RA-786.

(2) Gerwien, A.; Schildhauer, M.; Thumser, S.; Mayer, P.; Dube, H. Direct Evidence for Hula Twist and Single-Bond Rotation Photoproducts. *Nat. Commun.* **2018**, *9* (1), 1–9. https://doi.org/10.1038/s41467-018-04928-9.

(3) Redwood, C.; Bayda, M.; Saltiel, J. Photoisomerization of Pre- and Provitamin D3 in EPA at 77 K: One-Bond-Twist, Not Hula-Twist. *J. Phys. Chem. Lett.* **2013**, *4* (5), 716–721. https://doi.org/10.1021/jz302108c.

(4) Fuß, W.; Kosmidis, C.; Schmid, W. E.; Trushin, S. A. The Photochemical Cis-Trans Isomerization of Free Stilbene Molecules Follows a Hula-Twist Pathway. *Angew. Chemie - Int. Ed.* **2004**, *43* (32), 4178–4182. https://doi.org/10.1002/anie.200454221.

(5) Liu, R. S. H.; Hammond, G. S. The Case of Medium-Dependent Dual Mechanisms for Photoisomerization: One-Bond-Flip and Hula-Twist. *Proc. Natl. Acad. Sci.* **2000**, *97* (21), 11153–11158. https://doi.org/10.1073/pnas.210323197.

(6) Fuß, W. Previtamin D: Z-E Photoisomerization via a Hula-Twist Conical Intersection. *Phys. Chem. Chem. Phys.* **2019**, *21* (13), 6776–6789. https://doi.org/10.1039/c9cp00500e.

(7) Saltiel, J.; Krishna, T. S. R.; Clark, R. J. Photoisomerization of Cis,Cis-1,4-Diphenyl-1,3-Butadiene in the Solid State: The Bicycle-Pedal Mechanism. *J. Phys. Chem. A* **2006**, *110* (5), 1694–1697. https://doi.org/10.1021/jp056700d.

(8) Saltiel, J.; Krishna, T. S. R.; Laohhasurayotin, S.; Fort, K.; Clark, R. J. Photoisomerization of Cis , Cis - to Trans , Trans -1,4-Diaryl-1,3-Butadienes in the Solid State: The Bicycle-Pedal Mechanism. *J. Phys. Chem. A* **2008**, *112* (2), 199–209. https://doi.org/10.1021/jp077342c.

(9) Furukawa, D.; Kobatake, S.; Matsumoto, A. Direct Observation of Change in the Molecular Structure of Benzyl (Z,Z)-Muconate during Photoisomerization in the Solid State. *Chem. Commun.* **2008**, No. 1, 55–57. https://doi.org/10.1039/b714792a.

(10) Odani, T.; Matsumoto, A.; Sada, K.; Miyata, M. One-Way EZ-Isomerization of Bis(n-Butylammonium) (Z,Z)-Muconate under Photoirradiation in the Crystalline State. *Chem. Commun.* **2001**, *19* (c), 2004–2005. https://doi.org/10.1039/b106155k.

(11) Saltiel, J.; Bremer, M. A.; Laohhasurayotin, S.; Krishna, T. S. R. Photoisomerization of Cis,Cis- and Cis,Trans-1,4-Di-o-Tolyl-1,3-Butadiene in Glassy Media at 77 K: One-Bond-Twist and Bicycle-Pedal Mechanisms. *Angew. Chemie Int. Ed.* **2008**, *47* (7), 1237–1240. https://doi.org/10.1002/anie.200704465.

(12) Tong, F.; Al-Haidar, M.; Zhu, L.; Al-Kaysi, R. O.; Bardeen, C. J. Photoinduced Peeling of Molecular Crystals. *Chem. Commun.* **2019**, *55* (26), 3709–3712. https://doi.org/10.1039/c8cc10051a.

(13) Sonoda, Y.; Kawanishi, Y.; Tsuzuki, S.; Goto, M. Crystalline-State Z,E-Photoisomerization of a Series of (Z,E,Z)-1,6-Diphenylhexa-1,3,5-Triene 4,4'-Dicarboxylic Acid Dialkyl Esters. Chain

Length Effects on the Crystal Structure and Photoreactivity. *J. Org. Chem.* **2005**, *70* (24), 9755–9763. https://doi.org/10.1021/jo051137g.

(14) Saltiel, J.; Redwood, C. E.; Laohhasurayotin, K.; Samudrala, R. Photochemistry of the 1,6-Dideuterio-1,3,5-Hexatrienes in Solution: Efficient Terminal Bond Photoisomerization in One-Bond-Twist and Bicycle Pedal Ways. *J. Phys. Chem. A* **2018**, *122* (43), 8477–8489. https://doi.org/10.1021/acs.jpca.8b08288.

(15) Jung, Y. O.; Lee, J. H.; Kim, J.; Schmidt, M.; Moffat, K.; Šrajer, V.; Ihee, H. Volume-Conserving Trans–cis Isomerization Pathways in Photoactive Yellow Protein Visualized by Picosecond X-Ray Crystallography. *Nat. Chem.* **2013**, *5* (3), 212–220. https://doi.org/10.1038/nchem.1565.

(16) A, W. Bicycle-Pedal Model for First Step in Vision Process. *Nature* **1976**, *260*, 679.

(17) Saltiel, J.; Redwood, C. E. Photochemistry of the 1,4-Diphenyl-1,3-Butadienes in Ethanol. Trapping Conical Intersections. *J. Phys. Chem. A* **2016**, *120* (18), 2832–2840. https://doi.org/10.1021/acs.jpca.6b02330.

(18) Saltiel, J.; Bremer, M. A.; Laohhasurayotin, S.; Krishna, T. S. R. Photoisomerization of Cis,Cis- and Cis,Trans-1,4-Di-o-Tolyl-1,3-Butadiene in Glassy Media at 77 K: One-Bond-Twist and Bicycle-Pedal Mechanisms. *Angew. Chemie - Int. Ed.* **2008**, *47* (7), 1237–1240. https://doi.org/10.1002/anie.200704465.

(19) Olivucci, M.; Ragazos, I. N.; Bernardi, F.; Robb, M. A. A Conical Intersection Mechanism for the Photochemistry of Butadiene. A MC-SCF Study. *J. Am. Chem. Soc.* **1993**, *115* (9), 3710–3721. https://doi.org/10.1021/ja00062a042.

(20) Kuhlman, T. S.; Glover, W. J.; Mori, T.; Moller, K. B.; Martínez, T. J. Between Ethylene and Polyenes - The Non-Adiabatic Dynamics of Cis-Dienes. *Faraday Discuss.* **2012**, *157*, 193–212. https://doi.org/10.1039/c2fd20055d.

(21) Glover, W. J.; Mori, T.; Schuurman, M. S.; Boguslavskiy, A. E.; Schalk, O.; Stolow, A.; Martínez, T. J. Excited State Non-Adiabatic Dynamics of the Smallest Polyene, Trans 1,3-Butadiene. II. Ab Initio Multiple Spawning Simulations. *J. Chem. Phys.* **2018**, *148* (16). https://doi.org/10.1063/1.5018130.

(22) Ogliaro, F.; Wilsey, S.; Bearpark, M. J.; Sardo-Infirri, S. Interpreting the Excited States and Decay Processes of Bichromophoric 1-Phenyl-1,3-Butadiene Using CASSCF Calculations. *Mol. Phys.* **2006**, *104* (5–7), 1017–1032. https://doi.org/10.1080/00268970500418307.

(23) Norton, J. E.; Houk, K. N. H/Vinyl Conical Intersections of Hexatrienes Related to the Hula-Twist Photoisomerization. *Mol. Phys.* **2006**, *104* (5–7), 993–1008. https://doi.org/10.1080/00268970500417606.

(24) Sampedro Ruiz, D.; Cembran, A.; Garavelli, M.; Olivucci, M.; Fuß, W. Structure of the Conical Intersections Driving the Cis–trans Photoisomerization of Conjugated Molecules. *Photochem. Photobiol.* **2002**, *76* (6), 622. https://doi.org/10.1562/0031-8655(2002)076<0622:SOTCID>2.0.CO;2.

(25) Wilsey, S.; Houk, K. N. H-Vinyl Conical Intersections for Dienes: A Mechanism for the Photochemical Hula Twist. *Photochem. Photobiol.* **2002**, *76* (6), 616–621. https://doi.org/10.1562/0031-8655(2002)076<0616:HVCIFD>2.0.CO;2.

(26) Zimmerman, H. E.; Sebek, P.; Zhu, Z. Ab Initio Computations of Reacting Species in Crystal Lattices; Mechanistic and Exploratory Organic Photochemistry [17]. *Journal of the American Chemical Society*. 1998, pp 8549–8550. https://doi.org/10.1021/ja980042b.

(27) Zimmerman, H. E.; Alabugin, I. V; Smolenskaya, V. N. Experimental and Theoretical Host-Guest Photochemistry; Control of Reactivity with Host Variation and Theoretical Treatment with a Stress Shaped Reaction Cavity; Mechanistic and Exploratory Organic Photochemistry. *Tetrahedron* **2000**, *56* (36), 6821–6831. https://doi.org/10.1016/S0040-4020(00)00504-4.

(28) Zimmerman, H. E.; Nesterov, E. E. Development of Experimental and Theoretical Crystal

Lattice Organic Photochemistry : The Quantitative Cavity . Mechanistic and Exploratory Organic. **2002**, *35* (2), 77–85. https://doi.org/10.1021/ar000210g.
(29) Ruiz-Barragan, S.; Morokuma, K.; Blancafort, L. Conical Intersection Optimization Using Composed Steps Inside the ONIOM(QM:MM) Scheme: CASSCF:UFF Implementation with Microiterations. *J. Chem. Theory Comput.* **2015**, *11* (4), 1585–1594. https://doi.org/10.1021/acs.jctc.5b00004.
(30) Bučko, T.; Hafner, J.; Lebègue, S.; Ángyán, J. G. Spin Crossover Transition of Fe(Phen)2(NCS)2: Periodic Dispersion-Corrected Density-Functional Study. *Phys. Chem. Chem. Phys.* **2012**, *14* (16), 5389–5396. https://doi.org/10.1039/c2cp40111h.
(31) Presti, D.; Labat, F.; Pedone, A.; Frisch, M. J.; Hratchian, H. P.; Ciofini, I.; Cristina Menziani, M.; Adamo, C. Modeling Emission Features of Salicylidene Aniline Molecular Crystals: A QM/QM' Approach. *J. Comput. Chem.* **2016**, *37* (9), 861–870. https://doi.org/10.1002/jcc.24282.
(32) Wilbraham, L.; Adamo, C.; Labat, F.; Ciofini, I. Electrostatic Embedding to Model the Impact of Environment on Photophysical Properties of Molecular Crystals: A Self-Consistent Charge Adjustment Procedure. *J. Chem. Theory Comput.* **2016**, *12* (7), 3316–3324. https://doi.org/10.1021/acs.jctc.6b00263.
(33) Rivera, M.; Dommett, M.; Crespo-Otero, R. ONIOM(QM:QM') Electrostatic Embedding Schemes for Photochemistry in Molecular Crystals. *J. Chem. Theory Comput.* **2019**, *15* (4), 2504–2516. https://doi.org/10.1021/acs.jctc.8b01180.
(34) Aldaz, C.; Wang, L.-P.; Martinez, T. J.; Zimmerman, P. M. A Linear Scaling Growing String Method with Correlated Motions, In Preparation. **2020**.
(35) Wang, L. P.; Song, C. Geometry Optimization Made Simple with Translation and Rotation Coordinates. *J. Chem. Phys.* **2016**, *144* (21), 214108. https://doi.org/10.1063/1.4952956.
(36) Zimmerman, H. E.; Nesterov, E. E. Crystal Lattice Photochemistry Often Proceeds in Discrete Stages. Mechanistic and Exploratory Organic Photochemistry 1 , 2. *Org. Lett.* **2000**, *2* (8), 1169–1171. https://doi.org/10.1021/ol0057838.
(37) Zimmerman, H. E.; Alabugin, I. V; Chen, W.; Zhu, Z.; June, R. V. Dramatic Effects of Crystal Morphology on Solid State Reaction Course; Control by Crystal Disorder; Mechanistic and Exploratory Organic Photochemistry. *J. Am. Chem. Soc.* **1999**, *121* (6), 11930–11931. https://doi.org/10.1021/ja992208u.
(38) Aldaz, C. https://github.com/ZimmermanGroup/pyGSM.
(39) Zimmerman, P. M. Growing String Method with Interpolation and Optimization in Internal Coordinates: Method and Examples. *J. Chem. Phys.* **2013**, *138* (18), 1–11. https://doi.org/10.1063/1.4804162.
(40) Zimmerman, P. M. Single-Ended Transition State Finding with the Growing String Method. *J. Comput. Chem.* **2015**, *36* (9), 601–611. https://doi.org/10.1002/jcc.23833.
(41) Dewyer, A. L.; Zimmerman, P. M. Finding Reaction Mechanisms, Intuitive or Otherwise. *Org. Biomol. Chem.* **2017**, 501–504. https://doi.org/10.1039/C6OB02183B.
(42) Aldaz, C.; Kammeraad, J. A.; Zimmerman, P. M. Discovery of Conical Intersection Mediated Photochemistry with Growing String Methods. *Phys. Chem. Chem. Phys.* **2018**, *20* (43), 27394–27405. https://doi.org/10.1039/C8CP04703K.
(43) Baker, J.; Kessi, A.; Delley, B. The Generation and Use of Delocalized Internal Coordinates in Geometry Optimization. *J. Chem. Phys.* **1996**, *105* (1996), 192–212. https://doi.org/10.1063/1.471864.
(44) Ufimtsev, I. S.; Martinez, T. J. Quantum Chemistry on Graphical Processing Units. 3. Analytical Energy Gradients, Geometry Optimization, and First Principles Molecular Dynamics. *J. Chem.*

Theory Comput. **2009**, *5* (10), 2619–2628. https://doi.org/10.1021/ct9003004.
(45) Hohenstein, E. G.; Luehr, N.; Ufimtsev, I. S.; Martínez, T. J. An Atomic Orbital-Based Formulation of the Complete Active Space Self-Consistent Field Method on Graphical Processing Units. *J. Chem. Phys.* **2015**, *142* (22). https://doi.org/10.1063/1.4921956.
(46) Isborn, C. M.; Götz, A. W.; Clark, M. A.; Walker, R. C.; Martínez, T. J. Electronic Absorption Spectra from MM and Ab Initio QM/MM Molecular Dynamics: Environmental Effects on the Absorption Spectrum of Photoactive Yellow Protein. *J. Chem. Theory Comput.* **2012**, *8* (12), 5092–5106. https://doi.org/10.1021/ct3006826.
(47) Eastman, P.; Swails, J.; Chodera, J. D.; McGibbon, R. T.; Zhao, Y.; Beauchamp, K. A.; Wang, L. P.; Simmonett, A. C.; Harrigan, M. P.; Stern, C. D.; Wiewiora, R. P.; Brooks, B. R.; Pande, V. S. OpenMM 7: Rapid Development of High Performance Algorithms for Molecular Dynamics. *PLoS Comput. Biol.* **2017**, *13* (7), 1–17. https://doi.org/10.1371/journal.pcbi.1005659.
(48) Levine, B. G.; Coe, J. D.; Martínez, T. J. Optimizing Conical Intersections without Derivative Coupling Vectors: Application to Multistate Multireference Second-Order Perturbation Theory (MS-CASPT2) †. *J. Phys. Chem. B* **2008**, *112* (2), 405–413. https://doi.org/10.1021/jp0761618.
(49) Levine, B. G.; Martínez, T. J. Isomerization through Conical Intersections. *Annu. Rev. Phys. Chem.* **2007**, *58*, 613–634. https://doi.org/10.1146/annurev.physchem.57.032905.104612.
(50) Levine, B. G.; Martínez, T. J.; Martı, T. J. Ab Initio Multiple Spawning Dynamics of Excited Butadiene: Role of Charge Transfer. *J. Phys. Chem. A* **2009**, *113* (46), 12815–12824. https://doi.org/10.1021/jp907111u.
(51) Saltiel, J.; Krishna, T. R. S.; Laohhasurayotin, K.; Ren, Y.; Phipps, K.; Davis, P. H.; Yee, W. A. Medium Effects on the Direct Cis-Trans Photoisomerization of 1,4-Diphenyl-1,3-Butadiene in Solution. *J. Phys. Chem. A* **2011**, *115* (11), 2120–2129. https://doi.org/10.1021/jp111482m.
(52) The Gas-Phase MECI Are below the S1 Minimum like the MECI for Butadiene, but Unlike the MECI for Phenylbutadiene Which Are above the S1 Minimum.
(53) Wang, B.; Wang, X.; Wang, W.; Liu, F. Exploring the Mechanism of Fluorescence Quenching and Aggregation-Induced Emission of a Phenylethylene Derivative by QM (CASSCF and TDDFT) and ONIOM (QM:MM) Calculations. *J. Phys. Chem. C* **2016**, *120* (38), 21850–21857. https://doi.org/10.1021/acs.jpcc.6b07963.
(54) Peng, X. L.; Ruiz-Barragan, S.; Li, Z. S.; Li, Q. S.; Blancafort, L. Restricted Access to a Conical Intersection to Explain Aggregation Induced Emission in Dimethyl Tetraphenylsilole. *J. Mater. Chem. C* **2016**, *4* (14), 2802–2810. https://doi.org/10.1039/c5tc03322e.
(55) Sumita, M.; Saito, K. Theoretical Study on Hula-Twist Motion of Penta-2,4-Dieniminium on the S1 Surface under Isolated Condition by the Complete Active Space Self-Consistent Field Theory. *Chem. Phys. Lett.* **2006**, *424* (4–6), 374–378. https://doi.org/10.1016/j.cplett.2006.04.093.
(56) Boggio-Pasqua, M.; Ravaglia, M.; Bearpark, M. J.; Garavelli, M.; Robb, M. a. Can Diarylethene Photochromism Be Explained by a Reaction Path Alone? A CASSCF Study with Model MMVB Dynamics. *J. Phys. Chem. A* **2003**, *107* (50), 11139–11152. https://doi.org/10.1021/jp036862e.

TOC Graphic